PS/LP Note 90-49
December 1990

Results from e^+ measurements at LIL in December 1989

H. Braun (PSI), J. Madsen, A. Riche and L. Rinolfi

Contents

1 Introduction

This note is a summary of some measurements and their results done during several machine developments, which took place between the 4th and 6th of December 1989.

2 Reproduction and optimization of a former set-up

2.1 Set back reference values of 25 August 1989

The LIL performances were measured under the existing settings at the beginning of the session. These settings were achieved during different optimizations and adjustments over the last months. The positron production read at HIP.UMA 22 was $8.0 \cdot 10^8$.

All reference values made on 25 August were set back (see table 1 for RF-parameters). The positron production at HIP.UMA 22 becomes $8.3 \cdot 10^8$ (Fig. 1). Two parameters have to be changed from the reference values:
i) The phase of modulators, mainly MDK 13.
ii) The current of VL.DQL152H.
This power supply was changed in order to allow the e- beam deflection with the new mechanism of the target. The resolved conversion efficiency is $3.1 \cdot 10^{-3}$.

2.2 Optimization with steering magnets

In order to compare with the previous measurement and to be sure that the klystron is in saturation the voltage of MDK03 was set to 26.2 kV, which gave a power of 13.3 MW (klystron output reading). The power in MDK 13 was raised to 24.0 MW with a klystron voltage of 35.1 kV (Fig. 2 and 3).

From this point several adjustments with steering dipoles were done. The idea was to vary the current pair by pair for a given plane on an experimental basis and also to try to set the currents close to zero. Fig. 4 gives the horizontal current values. If at the end of LIL-W, the currents are close to nut, upstream and downstream of the target, there are far from small values.

Fig. 5 shows the vertical current values. Except just downstream of the target, almost all values are close to zero. One power supply upstream the target is also different of zero. The geometry downstream the target is probably not very well adjusted. Some efforts should be devoted to this part of the machine. The focussing of the linac was not changed. Fig. 6 gives the current values.

After the optimization of the steering the positron production raised from 8.3 to $12.0 \cdot 10^8$ e^+ per pulse.

2.3 Fluctuations of HIP.UMA 22

During a few minutes, the positron production was recorded. Fig. 7 shows the results. Table 2 summarizes the observation.

signal HIP.UMA 22	Sigma (10^8)	Delta H (mV)	Delta V (mV)
1	11.9	9.1	- 0.3
2	12.0	8.1	- 0.3
3	12.1	7.8	- 0.3

Table 2:

The vertical position does not change. When Delta H decreases by 1.3 mm, Sigma increases by $2 \cdot 10^7 e^+$. From tab. 2 one gets a short term stability of $\frac{0.2}{12.0} = 0.02$.

2.4 Phase adjustment

With Uc = 1.68 kV on the gun, providing $3.6 \cdot 10^{11} e^-$ at ECM 01, each modulator has been optimized. With phases displayed on figure 8, the positron intensity rises up to $12.4 \cdot 10^8$ (Fig. 9). Only the phase of MDK31 was changed from 214 deg. to 200 deg. . Fig. 10 displays the beam profile at the end of LIL-V.

2.5 Optimum of Uc

Fig. 11 shows the variation of UMA 15 and HIP.UMA 22 vs. Uc. The maximum is obtained when Uc = 1.95 kV. With this value, UMA 15 reads $2.5 \cdot 10^{11} e^-$ and HIP.UMA 22 reads $14.3 \cdot 10^9 e^+$ (Fig. 12). A scan with the phase between the prebuncher and the buncher was done. The maximum is always when the phase equals 42 digits.

2.6 Increase of MDK03 power

The maximum intensity on UMA15 and HIP UMA22 is obtained when P(03)=13.8 MW. This klystron output reading is get with a klystron voltage of 26.4kV (Fig.13). It provides $3.0 \cdot 10^{11} e^-$ on UMA 15 and $17.1 \cdot 10^8 e^+$ on HIP 22 unresolved (Fig.14 and 15).

2.7 Conversion efficiency

Fig. 16 displays the measured positrons per pulse resolved which is $12.9 \cdot 10^8$. With slits closed at 17 mm, the energy dispersion is $\pm 1\%$ and the maximum is obtained when the position of the slits is X = + 4mm.

The resolved conversion efficiency is $\frac{12.9}{3000} = 0.0043$.

2.8 Conclusions from the measurements of this section

The design value of resolved efficiency is reached. However, a comparison with SLAC value shows that a factor 3 could be gain. A simulation of the positrons production indicates that a factor 5 is missing with a correct geometry downstream the target and a correct value of the focussing solenoid SNP 25. Other studies are proposed to increase the positron production:

1. Beam loading in the cavities.

2. Transversal positions of solenoids downstream the target.

3. Optics of the linacs.

1. Systematic check of the LHL-W acceptance for positrons.

3 Tests related to section 25/26 magnet coils

3.1 Test of new steering method

We changed the settings of the correction dipoles on ACS25/26 from the settings in column 1 of tab. 3 to a set of values (column 2 in tab. 3) found with a new method, which uses the 220 MeV electron beam to adjust the coil currents [1]. The positron current dropped from $8.9 \cdot 10^8$ to $5.8 \cdot 10^8$, but could be raised to $8.2 \cdot 10^8$ by readjusting the e^- beam position on the target and some of the ACS25/26 correctors (column 3 of tab. 3). It is remarkable that roughly the same yield can be obtained with two completely different settings of the steering coils.

Corrector	initial val.	val. from [1]	optimized
DHG 251	-4.8 A	-12.5 A	-13.0 A
DHG 252	-17.9 A	-12.0 A	-20.0 A
DHG 261	-19.5 A	-20.0 A	-20.0 A
DHG 262	-9.8 A	-20.0 A	-20.0 A
DVG 251	0.0 A	-9.8 A	-10.0 A
DVG 252	17.4 A	6.8 A	6.8 A
DVG 261	8.8 A	13.0 A	13.0 A
DVG 262	8.3 A	6.0 A	6.0 A
HIP22($\cdot 10^8$)	8.9	5.8	8.2

Table 3: Corrector settings for ACS25/26 correctors

3.2 Test of the sensitivity of ACS25 steering coils

The dependence of the energy resolved e^+ current on HIP22 from the correction coil currents was recorded (Tab. 4). It turned out, that the dependence is not very strong (which may also explains the results of the section before), nevertheless the results are not very precise, since there was a drift of the e^+ yield during the measurements and also a control problem with DVG251.

3.3 Scan of pulsed coil SNP25 current

The resolved e^+ current vs. I_{snp25} was measured. For the results see tab. 5. The variation of the solenoid SNP 25 is still without a big effect on the e^+ production contrarily to what is expected from calculations.

Although it is designed to take a maximum current of 6000 A the optimum yield is obtained at less than half of this current. Switching the solenoid off reduces the yield by a factor of two. Later on it has been shown that the drop is a factor 3 when a fine optimization of the yield was done.

DHG251 A	DVG251 A	DHG252 A	DVG252 A	HIP22 10^8
-1.2	0.0	-18.0	+19.0	7.7
+20.0	0.0	-18.0	+19.0	5.7
-1.2	0.0	-18.0	+10.0	5.1
-1.2	0.0	-18.0	+7.0	3.8
-1.2	10.0	-18.0	+19.0	4.5
-1.2	-10.0	-18.0	+19.0	4.7
-1.2	0.0	+20.0	+19.0	3.5
-1.2	0.0	-18.0	+19.0	6.9

Table 4: Resolved e^+ yield ($\pm 1\%$) for different steering coil settings

I_{SNP25} [A]	HIP22 [$\cdot 10^8$]
0	2.9
1000	4.9
1500	5.3
2000	5.6
2500	5.8
3000	5.5
3500	5.3

Table 5: HIP22 vs. I_{SNP25}.

4 Scans of RF-parameter

4.1 Dependence of e^+-yield from the phase of LINAC V relative to LINAC W

The phase of LINAC V was varied relative to the phase of LINAC W by changing the phases MDK03 and MDK13 simultaneously. The value for $MDK13$ is $MDK03 + 195°$ in these measurements. The yield was measured with HIP22 (Fig. 17). The width of collimator HIP.SLH20 was reduced to 17 mm corresponding to a $\pm 1\%$ energy acceptance. For each setting of the phases the position of HIP.SLH20 was optimized for optimum yield. (Remark: The graphical display of the collimator position didn't work satisfactory). On 5th of Dec. a scan over 360° was done. The measurement was redone for the decelerating regime one day later after the machine was optimized for higher e^+ production. It should be mentioned that the steering was done for the decelerating mode and not changed during the measurement, thus the values in the accelerating mode are far away from optimum.

4.2 Measurement of LINAC V spectrum

The energy spectrum of LINAC V was measured for different settings of MDK03 (Fig. 18-21). The value of $MDK13$ was fixed to 308° during these measurements. The aim of this measurement was to get an estimate of the LINAC V microbunchlength (section 5). For

this measurement the beamloading was reduced by changing the pulse length of the gun from $20\,nsec$ to $12\,nsec$. The beam intensity on the target was $1.8 \cdot 10^{11}$ part. p. pulse before the reduction of the pulse length, therefore is in the next section a pulsecharge of $\frac{12}{20} \cdot 1.8 \cdot 10^{11}$ particles assumed.

4.3 Variation of ACS25/26 field strength

The field strength was changed by variation of the power of klystron 25. The e^+ yield showed a strong dependence (Tab. 6). But one has to be careful about this results, the r.f.-phase of klystron 25 which presumably depends strongly on the power, was not checked during these measurements since we ran out of time.

$P_{Kly.25}$ MW	$HIP22$ 10^8
18.1	8.0
17.4	6.8
18.8	3.5

Table 6: HIP22 signal for different klystron 25 output powersettings

5 Determination of LINAC V bunchlength

The aim of this chapter is to give an estimate of the bunchlength of Linac V. The Monte-Carlo Simulation of the positron capture system shows that especially in the decelerating mode the LIL positron yield is very sensitive to the bunchlength of Linac V. Therefore a realistic value of the bunchlength is essential to get simulation results which are comparable with measurements. On the other hand a method for the measurement of the bunchlength could be used for its minimization, leading to higher positron yields.

The method described is based on the idea, that the spectrum at the end of Linac V is mainly determined by beamloading and the phase distribution in the bunch at the end of the Linac V buncher. Additionally it is assumed, that the phase motion between the buncher and the end of Linac V is negligible. The limits of this simplification are discussed in Section 5.3. The spectra computed for different bunchlengths are then compared with the measured one, and the computed spectrum which fits best the measured spectrum is assumed to represent the right bunchlength.

5.1 Calculation of the spectra

The energy at the end of the linac depends on the initial phase of the electrons φ according to

$$T = T_0 + A\cos\varphi \approx T_0 + A(1 - \frac{\varphi^2}{2}) \tag{1}$$

With T_0 = kin. energy at the output of the buncher. Since only particles near the crest of the wave are taken into consideration, the approximation in (1) is valid. Assuming a parabolic bunch distribution

$$\frac{dn}{d\varphi} = \begin{cases} \frac{3}{4\sigma}(1 - \frac{(\varphi-\varphi_s)^2}{\sigma^2}) & \text{if } |\varphi - \varphi_s| \le \sigma \\ 0 & \text{otherwise} \end{cases} \tag{2}$$

with σ=half bunchlength and φ_s=phase of reference particle. The energy distribution is given by

$$\begin{aligned} \frac{dn}{dT} &= \frac{dn}{d\varphi}\frac{d\varphi}{dT} \\ &= \frac{3}{4\sigma}(1 - \frac{(\varphi-\varphi_s)^2}{\sigma^2})\frac{1}{A\sqrt{2}\sqrt{1-\frac{T-T_0}{A}}} \\ &= \frac{3}{4\sigma}(1 - \frac{(\sqrt{2}\sqrt{1-\frac{T-T_0}{A}} - \varphi_s)^2}{\sigma^2})\frac{1}{A\sqrt{2}\sqrt{1-\frac{T-T_0}{A}}} \\ &\quad \text{if } |\sqrt{2}\sqrt{1-\frac{T-T_0}{A}} - \varphi_s| \le \sigma \\ &= 0 \text{ otherwise} \end{aligned} \tag{3}$$

Evaluating (3) in the case $\varphi - \sigma < 0$ one has to add the two possible values of (3) according to the two possible solutions of the roots.

The spectrum is broadened by beamloading. If the pulse length is very small compared to the filling time of the r.f. sections the spectrum changes according to

$$\frac{dn}{dT_{b.l.}}(T) = \frac{1}{\Delta T}\int_{T}^{T+\Delta T}\frac{dn}{dT}(\tau)\,d\tau \tag{4}$$

where the energy spread is approximately given by

$$\Delta T_{b.l.} \approx \frac{\omega_{rf}\,q\,T}{2\,Q}\sqrt{\frac{r\,L}{P}} \tag{5}$$

(Q=unloaded Quality factor, r=shunt impedance, L=length of a section, P=r.f. pulse power per section, q=charge of the pulse)
Inserting (3) in (4) yields

$$\begin{aligned}\frac{dn}{dT_{b.l.}}(T) &= \frac{1}{\Delta T}\int_{T}^{T+\Delta T}\frac{3}{4\sigma A}\left(1-\frac{(\sqrt{2}\sqrt{1-\frac{\tau-T_0}{A}}-\varphi_s)^2}{\sigma^2}\right)\frac{1}{\sqrt{2}\sqrt{1-\frac{\tau-T_0}{A}}}\,d\tau \\ &= \frac{3}{2\sqrt{2}\,\sigma^3}\left[\sigma^2-\frac{2}{3}u^3+\varphi_s\sqrt{2}\,u^2-\varphi_s u\right]_L^H \end{aligned}\tag{6}$$

with $L=\sqrt{1-\frac{T_{low}-T_0}{A}}$, $H=\sqrt{1-\frac{T_{high}-T_0}{A}}$ and $u=\sqrt{1-\frac{T-T_0}{A}}$, where the integration limits T_{low} and T_{high} has to be carefully chosen in the different cases caused by the condition in (2) and the condition that T cannot be bigger than T_0+A.

The energy spread of the buncher m_b and the resolution of the spectrometer m_r also acts on the measured spectra. This can be described by a convolution of (4) with a gaussian.

$$\frac{dn}{dT}(T)_{measured} = \frac{1}{\sqrt{2\pi}m}\int_{-\infty}^{+\infty}\frac{dn}{dT_{b.l.}}(\tau)\,e^{-\frac{(T-\tau)^2}{m^2}}\,d\tau \tag{7}$$

with $m=\sqrt{m_r^2+m_b^2}$.

5.2 Estimation of the systematic error of the calculation

Hitherto it was assumed, that the phase of the particles is "frozen" between the buncher and the end of Linac V, which is actually wrong. Due to the different momenta of different particles one has different particle velocities. The velocity deviation from the reference particle is given by

$$\frac{dv}{v} = \frac{1}{\gamma^2}\frac{dp}{p} \tag{8}$$

since $v\approx c$ this results in a phase error

$$\Delta\varphi = \frac{\omega\,L}{c\,\gamma^2}\frac{\Delta p}{p} \tag{9}$$

the magnitude of the error in the calculation of the energy δT can therefore be estimated

$$\begin{aligned}\delta T &= A\sin\varphi\,\Delta\varphi \\ &\approx A\,\varphi\,\frac{\omega L}{c\gamma^2}\frac{\Delta p}{p} \\ &= A\sqrt{2}\sqrt{1-\frac{T-T_0}{A}}\,\frac{\omega\,L}{c\gamma^2}\,\frac{\Delta p}{p}\end{aligned}\tag{10}$$

Evaluation of (10) shows, that the error vanishes for particles with the maximum energy. For a worst case estimation one has to take the $\frac{\Delta p}{p}$ and γ values at the end of the buncher. Inserting $\frac{\Delta p}{p} = 0.12$ (from [2] for $50\,nC$ pulse charge), $\gamma = 51$, $T_0 = 26\,MeV$, $L = 24\,m$, $\frac{\omega}{c} = 20\pi\,m^{-1}$ and $A = 194\,MeV$ one gets an error of $\delta T = 2.37\,MeV$ at $T = 217\,MeV$ and $\delta T = 4.33\,MeV$ at $T = 210\,MeV$ for example. Therefore a coincidence between the calculated and the measured spectra is only expected at the high energy end of the spectra.

5.3 Results

In figure 22 the measured spectra (see section 4) are compared to curves computed with (7) for $\sigma = 10°$, $20°$ and $30°$. In the computation a total beam loading of 5.5%, $m_r = 1.7\,MeV$ and $m_b = 1\,MeV$ is assumed. $MDK13$ was set to 308° during the measurements. With this adjustment a buncher phase of $MDK03 = 115°$ corresponds to an acceleration on the crest of the r.f. wave. At the high energy end of the spectra the measured spectra fits best with the curves computed with $\sigma = 20°$, therefore a total bunchlength of 40° seems to be a realistic estimate for the bunchlength of Linac V. It should be noted that the ability to vary the phase of one or two sections at the high energy end of the Linac V would allow a much more precise determination of the bunchlength. The systematic error described in section 3 would be drastically reduced, thus allowing a complete reconstruction of the bunch shape by a deconvolution method. The arbitrary assumption of a parabolic bunch shape (chosen to simplify the calculation described above) would be no longer needed.

References

[1] J. Madsen, "Tests during critical day 30 Nov. 89" CERN Nov. 1989

[2] P. Prunet, R. Chaput, "LIL front end, description and experimental results", Linear accelerator Conf., Darmstadt 1984

LIL RF REFERENCE SHEET

DATE = 21 AOUT 1989 TIME = 19h30 NAME = B. CAHARD

MDK/KLY	Booster	03	13	25	27	31	35	
Reading Peak Power	0.012	14.4	24	19.7	18.2	19.9	16	MW
Meter	20 kW	13.2	24.2	19	18,2	19,2	15,1	MW
KLY current		170	250	200	206	197	213	A
PFN		26.2	35	32,5	32	30	32	kV
PPi (V)		0.84	0,70	1,2	1,83	1,6	1,7	V
PKI (V)	1,5	2	0.66	1,8	2	1,6	0,96	V
LBNV or PSI-1 (V)		0.7	0,9	1,6	0,5	1,85	1,32	V
(2N values RF-PHASE (°RF)	e⁻	136	323	136	203	230	236	
	e+	133	341					
T.(°C)		32.3	29.8	29.8	30.6	29.0	28.8	
		32	29.9	29.8	30,6	29	28,9	
SKLY	29 874	29 901	29 885	29 941	29 870	29 880	29 937	
	29874	29901	29885	29941	29870	29880	29937	
SRFP		29 959	29 919	///	29 926	29 924	///	
		29959	29919	///	29926	29924	///	
ERFP		30009	30006		30014	30 012		
		30.009	30.006		30.014	30.012		
SRFI Coarse	e⁻		29986		29999	29973		
	e+		29986		29991	29981		
(Fine	e⁻		50		40	30		
	e+		6		30	31		
LBNV or PSI-1 Pulse length	5.5	4	4.5	3.5	4.5	4.5	3.5	µs
Base	5.5	4.5	4,5	3,5	4,6	4.5	3,5	

PBV PHASE = 41 à 43 Booster klystron = ~~LAt~~ . THOMSON

PBV ATTENUATOR = 43 à 43

TIMING GUN V Coarse = 30.000 Fine = 36

ALL MEASUREMENTS TO BE MADE IN KLYSTRON GALLERY AND AT ARROW:

Table 1

(1)

LIL UMA

1989-12-05-21:10:38

TRAJ. POSITRONS

	Intensite(E8)	Horizontal(mm)	Vertical(mm)	
UMA 13	-1905.8	-1.8	-.2	
UMA 15	-1890.0	-.4	-.6	
UMA 22	-1853.3	1.0	-.4	
UMA 25	-1874.1	.6	-.8	
UMA 27	-13.2	.1	-.2	
UMA 29	3.0	.1	.8	
UMA 30	6.1	-5.2	-1.5	WCH Intens.(E8)
UMA 31	6.9	-.1	-1.1	
UMA 32	6.2	1.6	-1.2	ECH01 -3645.8
UMA 33	6.8	-2.1	-1.3	WCH11 -2300.5
UMA 34	6.7	-2.9	-1.2	WCH12 -1929.0
UMA 35	5.8	-6.5	.5	WCH14 -1874.8
UMA 36	7.0	.1	.1	WCH37 6.4
UMA 37	7.5	.6	.4	HIP00 9.4
HIH 00	0.0	111.1	111.1	
HIE 22	0.0	111.1	111.11	
HIP 22	8.3	4.7	-.8	NMEAS 95

Fig 1

PLS POSIT 1989-12-05-22:14:44

POWER SUPPLIES FOR LPI OPERATION

FEC	EQN	OB.NAME	STATUS	CCV	AQN
LIL	6	VL.DHG031	ON	2.50	2.48
LIL	8	VL.DHG032	ON	2.70	2.69
LIL	41	VL.DHZ11	ON	.69	.70
LIL	43	VL.DHG1199	ON	-.50	-.50
LIL	49	VL.DQS121H	ON	5.20	5.20
LIL	53	VL.DHZ25	ON	1.99	1.99
LIL	57	VL.DQS132H	ON	-.20	-.20
LIL	63	VL.DQS141H	ON	6.58	6.56
LIL	65	VL.DHZ14	ON	5.00	4.99
LIL	67	VL.BSP15	STBY	253.49	.42
LIL	68	VL.DQL152H	ON	-2.99	-3.02
LIL	76	WL.DHG251	ON	-1.20	-1.17
LIL	78	WL.DHG252	ON	-18.20	-18.05
LIL	81	WL.DHG261	ON	-19.49	-19.45
LIL	83	WL.DHG262	ON	-9.99	-9.83
LIL	92	HI.BSH00	ON	173.50	173.74
LIL	96	WL.DQL272H	ON	-4.99	-5.02
LIL	98	WL.DQNF271H	XXXXX	-3.19	-3.20
LIL	102	WL.REC27	ON	0	0
LIL	103	WL.DQL28H	XXXXX	4.00	4.01
LIL	105	WL.DQNF284H	XXXXX	0	0
LIL	107	WL.DQNF292H	XXXXX	0	0
LIL	110	WL.REC28	ON	0	0
LIL	112	WL.DQNF302H	XXXXX	0	0
LIL	114	WL.DQNF313H	XXXXX	0	0
LIL	118	WL.REC30	ON	0	0
LIL	119	WL.DQNF331H	XXXXX	0	0
LIL	121	WL.DQNF342H	XXXXX	0	0
LIL	123	WL.DQNF362H	ON	1.00	1.00
LIL	126	WL.REC33	ON	0	0
LIL	133	HI.BHZ	ON	386.07	386.19

LiL Horizontal plane

Fig 4

PLS POSIT 1989-12-05-22:13:47

POWER SUPPLIES FOR LPI OPERATION

FEC	EQN	OB.NAME	STATUS	CCV	AQN
LIL	7	VL.DVG031	ON	.20	.20
LIL	9	VL.DVG032	ON	.20	.20
LIL	42	VL.DVT11	ON	-.50	-.50
LIL	44	VL.DVG1199	ON	0	0
LIL	47	VL.DQL12V	ON	0	0
LIL	54	VL.DVT25	ON	0	0
LIL	55	VL.DQL13V	ON	0	0
LIL	61	VL.DQL14V	ON	0	0
LIL	66	VL.DVT14	ON	-6.00	-5.99
LIL	69	VL.DQL153V	ON	0	0
LIL	77	WL.DVG251	ON	0	0
LIL	79	WL.DVG252	ON	19.00	18.95
LIL	82	WL.DVG261	ON	8.99	8.80
LIL	84	WL.DVG262	ON	8.50	8.33
LIL	95	WL.DQL271V	ON	0	0
LIL	97	WL.DQNM273V	XXXXX	0	0
LIL	99	WL.DQNF274V	XXXXX	0	0
LIL	102	WL.REC27	ON	0	0
LIL	104	WL.DQNF283V	XXXXX	0	0
LIL	106	WL.DQNF291V	XXXXX	1.99	2.01
LIL	110	WL.REC28	ON	0	0
LIL	111	WL.DQNF301V	XXXXX	0	0
LIL	113	WL.DQNF312V	XXXXX	.09	.09
LIL	115	WL.DQNF323V	XXXXX	0	.01
LIL	118	WL.REC30	ON	0	0
LIL	120	WL.DQNF341V	XXXXX	0	0
LIL	122	WL.DQNF361V	XXXXX	-1.00	-1.00
LIL	126	WL.REC33	ON	0	0
LIL	131	HI.DVT00	ON	65.93	65.93

LiL vertical plane

Fig 5

PLS POSIT 1989-12-05-22:16:14

POWER SUPPLIES FOR LPI OPERATION

FEC	EQN	OB.NAME	STATUS	CCV	AQN
LIL	1	VL.SNA01	ON	8.99	9.00
LIL	3	VL.SNC02	ON	12.20	12.19
LIL	4	VL.SNDE02	ON	112.9	112.92
LIL	5	VL.SNVU03	ON	70.10	70.13
LIL	10	VL.SNF11	ON	113.97	114.02
LIL	11	VL.QSA1212	ON	2.40	2.39
LIL	12	VL.QLA12	ON	2.70	2.66
LIL	13	VL.QSA1312	ON	2.40	2.38
LIL	14	VL.QLA13	ON	2.70	2.65
LIL	15	VL.QLA14	ON	4.19	4.19
LIL	16	VL.QSA1412	ON	3.39	3.39
LIL	17	VL.QLB1514	ON	57.00	57.01
LIL	18	VL.QLB1523	ON	53.6	53.56
LIL	36	VL.SNB02	ON	47.99	48.03
LIL	37	WL.SNP25	ON	2501.1	2536.26
LIL	38	WL.QLA271	ON	6.00	5.99
LIL	39	WL.QLA272	ON	8.98	8.98
LIL	40	WL.QLB2829	ON	55.00	55.03
LIL	75	WL.SNL25	ON	650.00	650.00
LIL	80	WL.SNL26	ON	650.00	649.94
LIL	85	WL.QNM271	ON	96.97	96.97
LIL	86	WL.QNM272	ON	106.5	106.5
LIL	87	WL.QNM273	ON	104.10	104.14
LIL	88	WL.QNFA	ON	135.99	135.99
LIL	89	WL.QNFB	ON	135.00	135.00
LIL	90	WL.QNFC	ON	128.99	129.03
LIL	91	WL.QNM36	ON	84.00	83.79
LIL	134	HI.QFD1	ON	96.41	96.45

LiL focusing

Fig 6

LIL UHA

1989-12-05-22:13:18

TRAJ. POSITRONS

	Intensite(EB)	Horizontal(mm)	Vertical(mm)		
UHA 13	-1916.4	-1.6	-.2		
UHA 15	-1895.3	-.2	-.6		
UHA 22	-1858.7	.8	-.3		
UHA 25	-1874.1	.7	0.0		
UHA 27	-10.2	2.3	1.7		
UHA 29	5.0	-7.5	.8		
UHA 30	8.0	-1.0	.4	WCH Intens.(EB)	
UHA 31	8.6	-1.4	-.8		
UHA 32	8.2	1.1	-2.3	EDH01	-3634.8
UHA 33	8.5	-.2	.3	WCH11	-2287.6
UHA 34	8.9	-.7	.7	WCH12	-1924.6
UHA 35	7.9	-4.8	-1.5	WCH14	-1883.4
UHA 36	9.0	.1	-1.3	WCH37	8.5
UHA 37	9.8	.6	-.8	HIP00	12.2
HIH 00	0.0	111.1	111.1		
HIE 22	-.3	111.1	111.11		
HIP 22	11.9	9.1	-.3	NMEAS	96

LIL UHA

1989-12-05-22:14:48

TRAJ. POSITRONS

	Intensite(EB)	Horizontal(mm)	Vertical(mm)		
UHA 13	-1916.4	-1.6	-.2		
UHA 15	-1895.3	-.3	-.6		
UHA 22	-1858.7	.8	-.3		
UHA 25	-1879.6	.7	0.0		
UHA 27	-10.2	2.3	1.7		
UHA 29	5.0	-7.0	.8		
UHA 30	8.0	-1.0	.4	WCH Intens.(EB)	
UHA 31	8.6	-1.4	-.8		
UHA 32	8.2	1.1	-2.3	EDH01	-3645.8
UHA 33	8.9	-.2	.3	WCH11	-2281.9
UHA 34	8.9	-.7	.7	WCH12	-1929.0
UHA 35	7.9	-4.8	-1.1	WCH14	-1887.7
UHA 36	9.4	.1	-1.2	WCH37	8.5
UHA 37	9.8	.6	-.8	HIP00	12.3
HIH 00	0.0	111.1	111.1		
HIE 22	-.3	111.1	111.11		
HIP 22	12.0	8.1	-.3	NMEAS	95

LIL UHA

1989-12-05-22:15:33

TRAJ. POSITRONS

	Intensite(EB)	Horizontal(mm)	Vertical(mm)		
UHA 13	-1911.1	-1.6	-.1		
UHA 15	-1895.3	-.3	-.5		
UHA 22	-1858.7	.8	-.3		
UHA 25	-1874.1	.7	0.0		
UHA 27	-10.2	2.3	1.7		
UHA 29	5.0	-7.0	.8		
UHA 30	8.0	-1.0	.4	WCH Intens.(EB)	
UHA 31	8.6	-1.4	-.8		
UHA 32	8.2	1.1	-2.3	EDH01	-3634.8
UHA 33	8.9	-.2	.3	WCH11	-2283.3
UHA 34	8.9	-.7	.7	WCH12	-1920.2
UHA 35	7.9	-4.8	-1.1	WCH14	-1879.1
UHA 36	9.4	.1	-1.3	WCH37	8.5
UHA 37	9.8	.6	-.8	HIP00	12.2
HIH 00	0.0	111.1	111.1		
HIE 22	-.3	111.1	111.11		
HIP 22	12.1	7.8	-.3	NMEAS	96

Fig 7

3)

0 H 20 6/12/1989

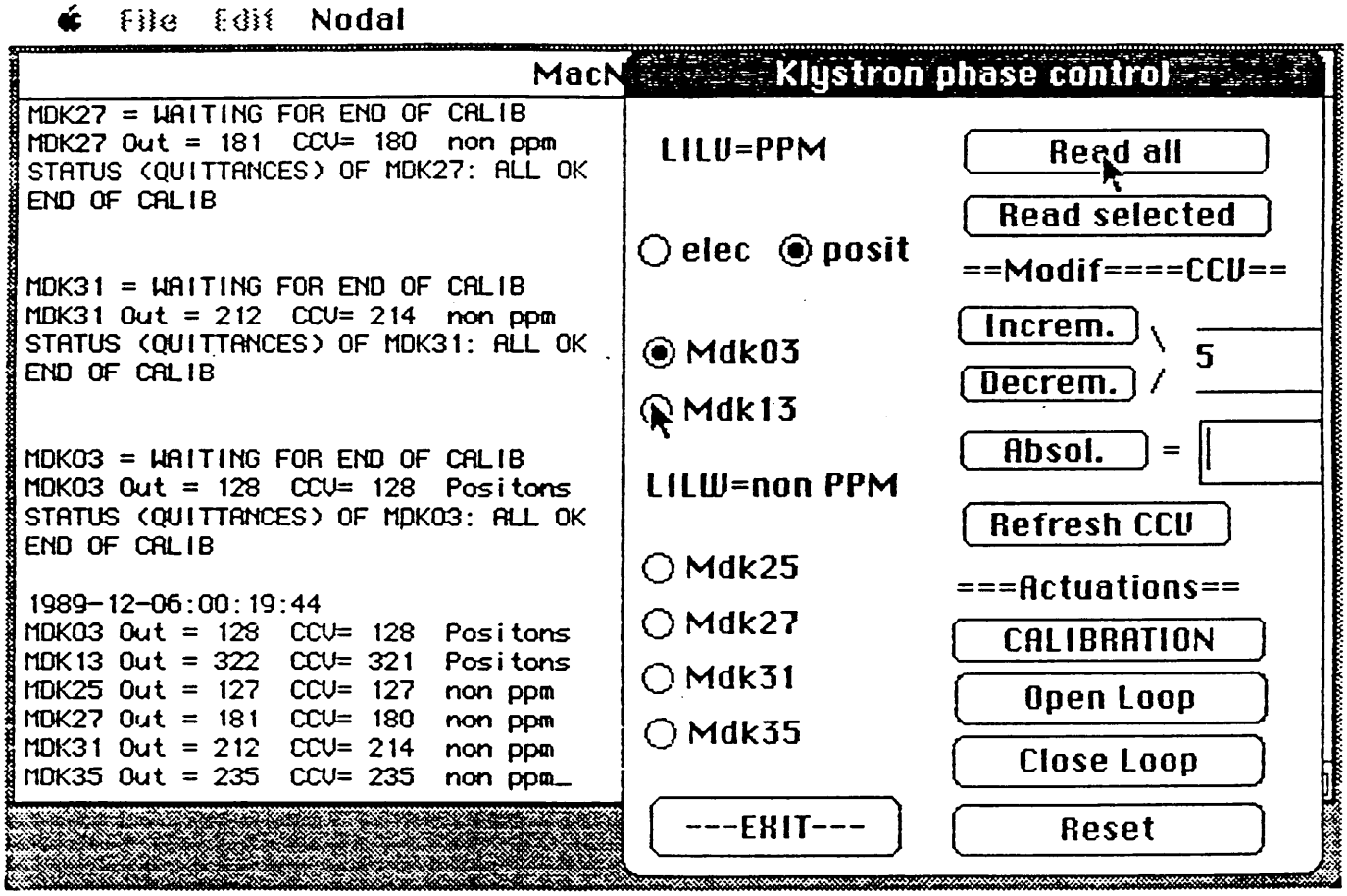

Fig 8

MDK 31 214° → 200° à 18 H

MDKU3 = 13.3 MW
MDK13 = 24 MW

(9)

LIL UMA

1989-12-05-22:32:24

TRAJ. POSITRONS

	Intensite(EB)	Horizontal(mm)	Vertical(mm)
UMA 13	-1911.1	-1.6	-.1
UMA 15	-1895.3	-.2	-.5
UMA 22	-1858.7	.8	-.3
UMA 25	-1879.6	.7	0.0
UMA 27	-10.2	2.3	1.7
UMA 29	5.0	-7.0	-1.3
UMA 30	8.3	-1.0	.4
UMA 31	8.9	-1.4	-.7
UMA 32	8.5	1.1	-2.1
UMA 33	8.9	-.2	.3
UMA 34	9.2	-.7	.7
UMA 35	8.2	-4.6	-1.0
UMA 36	9.4	.1	-1.2
UMA 37	10.2	.6	-.8
HIH 00	0.0	111.1	111.1
HIE 22	-.3	111.1	111.11
HIP 22	12.4	4.9	-.6

MCH	Intens.(EB)
ECH01	-3645.8
MCH11	-2274.7
MCH12	-1915.8
MCH14	-1879.1
MCH37	8.8
HIP00	12.5

NMEAS 95

Fig 9

CONSOLE - GRAPHIC SYSTEM HARD-COPY

05/DEC/1989-23:04:58
YVETTE CLPD

BEAM PROFILE MEASUREMENT - VL. MSH15

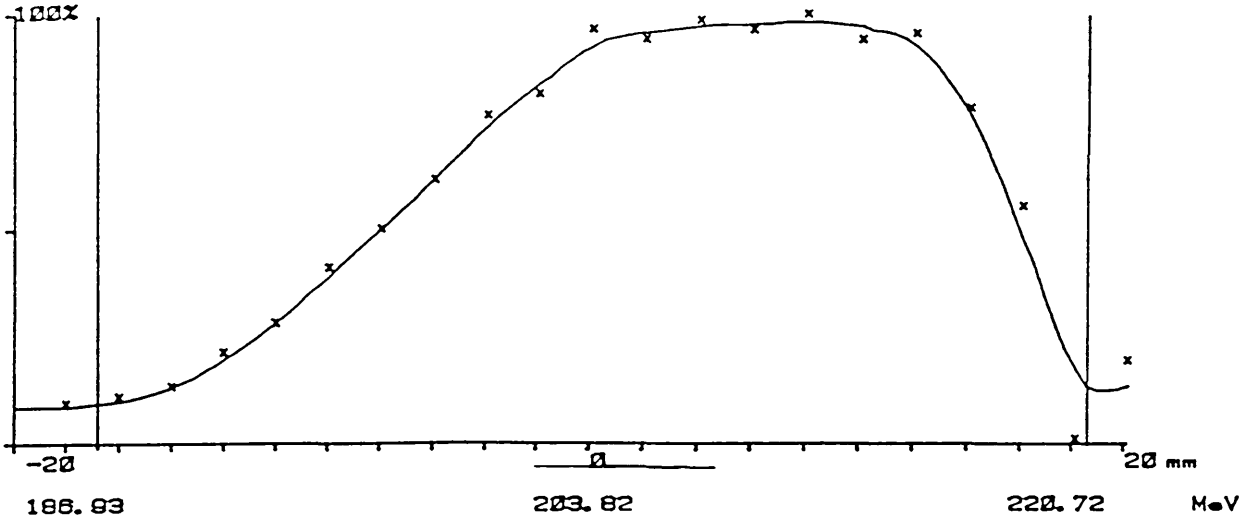

Central Energy 203.82 MeV

Digital Value at 100% 1448 (cal. 8047)

INTENSITY (UMA meas.) -124.88 1E8 part.

Number of measurements 100

2*sigma 17.89mm

Gain is .01

Scraper VL. SLV11 (Top) : -18.8(-18.5) mm

(Bottom) : 18.5(18.5) mm

BSP15 = 251.6 A

P_{03} = 13.3 MW

P_{13} = 24.0 MW

3

1000

HEWLETT-PACKARD 9280-0619 731

Fig 10

10

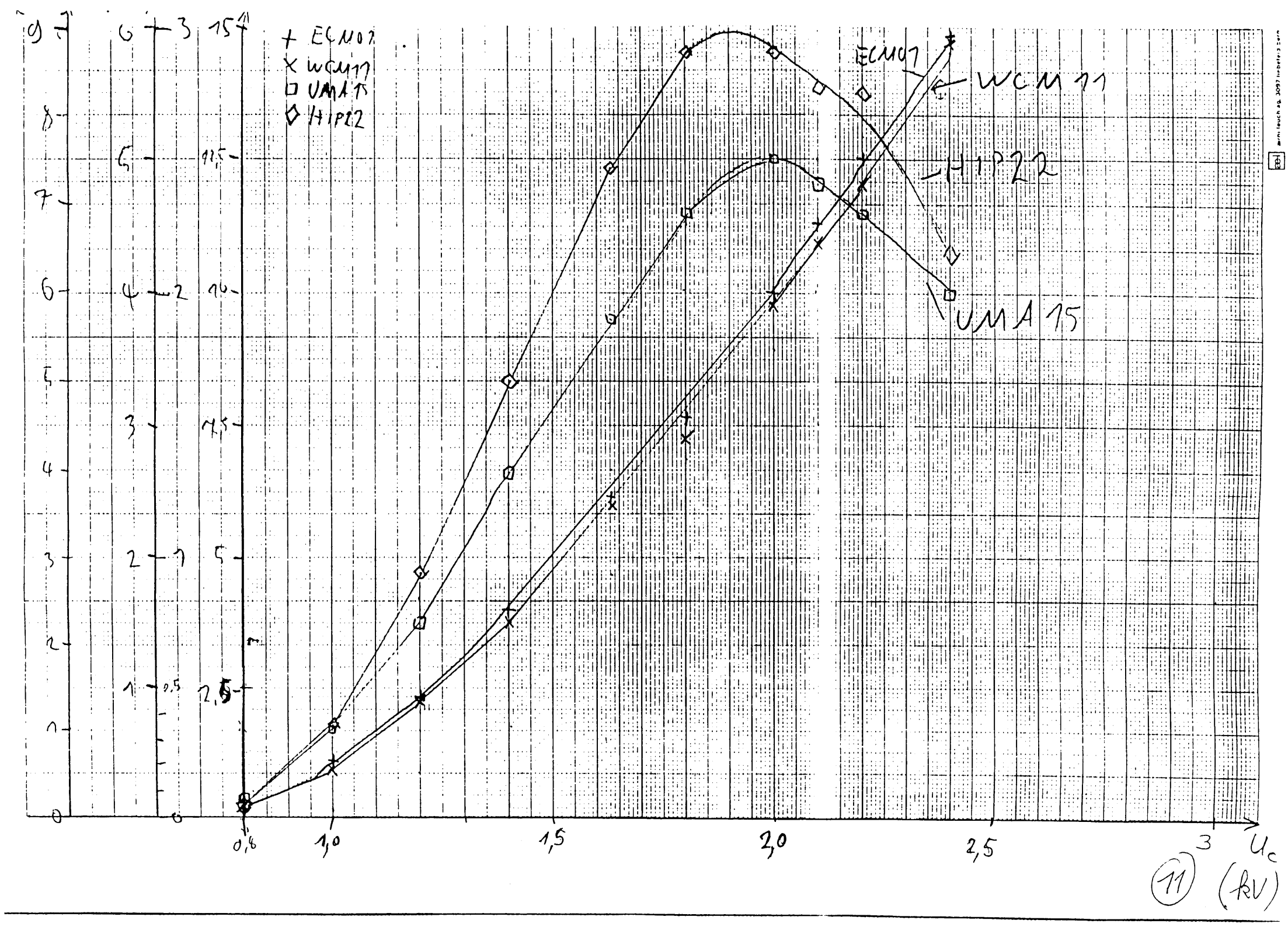
+ ECM07
× WCM11
□ UMA15
◇ HIP22
ECM07
WCM11
HIP22
UMA15
Q
G
I
U_c (kV)
0,6
1,0
1,5
2,0
2,5
3
11

(12)

$A_{PB} = 42$
$\varphi_{PB} = 42$
max value

LIL UMA

1989-12-06-08:27:05

TRAJ. POSITRONS

	Intensite(E8)	Horizontal(mm)	Vertical(mm)
UMA 13	-2927.6	-2.2	-.6
UMA 15	-2535.8	-1.3	-.8
UMA 22	-2412.0	0.0	-.6
UMA 25	-2429.2	.5	.1
UMA 27	-11.9	2.0	1.6
UMA 29	5.9	-5.8	.8
UMA 30	9.2	.3	.4
UMA 31	9.8	-1.2	-.6
UMA 32	9.8	.9	-1.8
UMA 33	10.0	-.2	1.5
UMA 34	10.2	-1.6	-.6
UMA 35	9.2	-4.1	-.9
UMA 36	10.7	.1	-1.1
UMA 37	11.1	.6	-.7
HIH 00	0.0	111.1	111.1
HIE 22	-.3	111.1	111.11
HIP 22	14.3	9.3	-.2

WCM	Intens.(E8)
ECH01	-5767.1
WCH11	-3715.2
WCH12	-3831.9
WCH14	-2786.4
WCH37	9.7
HIP00	14.7

NMEAS 95

Fig 12

(13)

MDK 03 PARAMETERS

1989-12-06-00:58:32

KLY BODY WATER IN TEMP	20.6 oC	THYR. RESERVE VOLTAGE	4.42 V
KL BODY WATER OUT TEMP	21.9 oC	THYR. RESERVE CURRENT	14.3 A
KLY TANK TEMPERATURE	35.7 oC	THYR. RESERVE POWER	60.9 W
SPARE		THYR. KEEP ALIVE VOLT	20.1 V
SPARE		THYR. KEEP ALIVE CUR	284 mA
SPARE		SPARE	
KLY FOCAL. A CURRENT	194.7 A	SPARE	
KLY FOCAL. B CURRENT	86.6 A	SPARE	
KLY FOCAL. C CURRENT	85.1 A	SPARE	
SPARE		SPARE	
KLY HEATER VOLTAGE	20.15 V	SPARE	
KLY HEATER CURRENT	20.6 A	SPARE	
KLY HEATER POWER	406 W	KLY. RF FORWARD POWER	13.8 MW
SPARE		PFN REF. VOLTAGE	26.4KV
PREHAGN CURRENT	17.3 A	KLYSTRON VOLTAGE	194 KV
KLY ION PUMP VOLTAGE	3.4kV	KLYSTRON CURRENT	172 A
KLY VACUUM PRESSURE	1E-8 Torr		
THYR. HEATER VOLTAGE	6.36 V		
THYR. HEATER CURRENT	62.3 A		
THYR. HEATER POWER	397 W		

Fig 13

(14) Unresolved I ... ces

LIL UMA

1989-12-06-01:09:31

TRAJ. POSITRONS

	Intensite(E8)	Horizontal(mm)	Vertical(mm)
UMA 13	-3102.3	-1.4	-.1
UMA 15	-2996.1	-.2	-.3
UMA 22	-2917.0	.9	-.1
UMA 25	-2940.4	.8	.3
UMA 27	-13.9	1.7	1.5
UMA 29	7.6	-6.1	-.6
UMA 30	11.3	-1.0	.4
UMA 31	12.2	-1.0	-1.3
UMA 32	12.1	.6	-1.3
UMA 33	12.5	-.2	1.2
UMA 34	12.7	-1.2	.7
UMA 35	12.0	-3.1	-.6
UMA 36	13.4	.1	-1.8
UMA 37	13.8	.6	-.4
HIH 00	0.3	111.1	111.1
HIE 22	-.6	111.1	111.11
HIP 22	17.1	8.4	-.4

WCH	Intens.(E8)
ECH01	-5678.7
WCH11	-3741.0
WCH12	-3132.9
WCH14	-3035.8
WCH37	12.3
HIP00	17.8

MMEAS 95

Fig 14

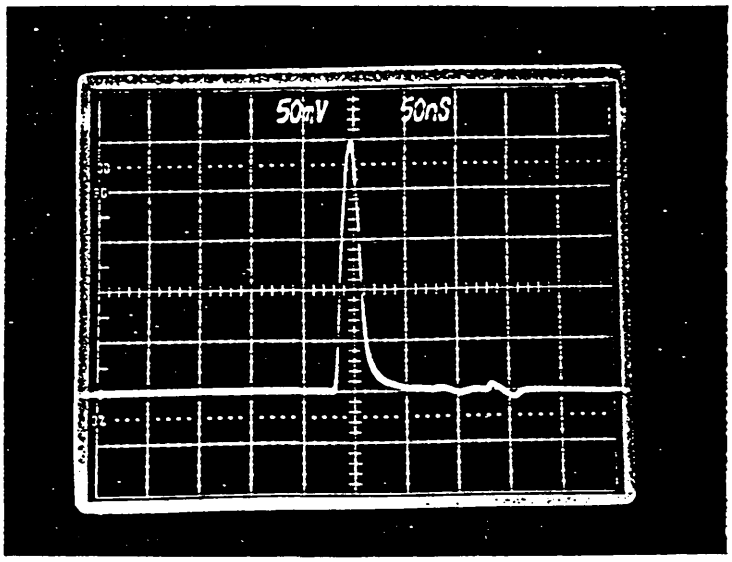

Fig 15 HIP. UMA 22

Analog value 250 mV

Digital value $17.4\ 10^{8}\ e^{+}$

for $U_c = 1.95$ kV
on the gun

(16) Resolved $P_0 = +4$ mm I max $\frac{\Delta E}{E} = \pm 1\%$

LIL UMA

1989-12-06-01:13:37

TRAJ. POSITRONS

	Intensite(E8)	Horizontal(mm)	Vertical(mm)
UMA 13	-3097.0	-1.3	0.0
UMA 15	-2991.1	-.2	-.3
UMA 22	-2911.6	1.0	0.0
UMA 25	-2940.4	.8	.3
UMA 27	-13.9	1.7	1.5
UMA 29	7.6	-6.1	-.6
UMA 30	11.6	-1.0	.4
UMA 31	12.5	-1.0	-.0
UMA 32	12.5	.6	-1.2
UMA 33	12.8	-.2	1.2
UMA 34	13.0	-1.2	.7
UMA 35	12.0	-3.1	-.6
UMA 36	13.4	.1	-1.7
UMA 37	14.1	.6	-.4
HIH 00	.3	111.1	111.1
HIE 22	-.6	111.1	111.11
HIP 22	12.9	4.3	-.8

MCH	Intens.(E8)
ECH01	-5678.7
MCH11	-3732.4
MCH12	-3128.5
MCH14	-3031.5
MCH37	12.5
HIP00	12.1

NMEAS 95

Fig 16

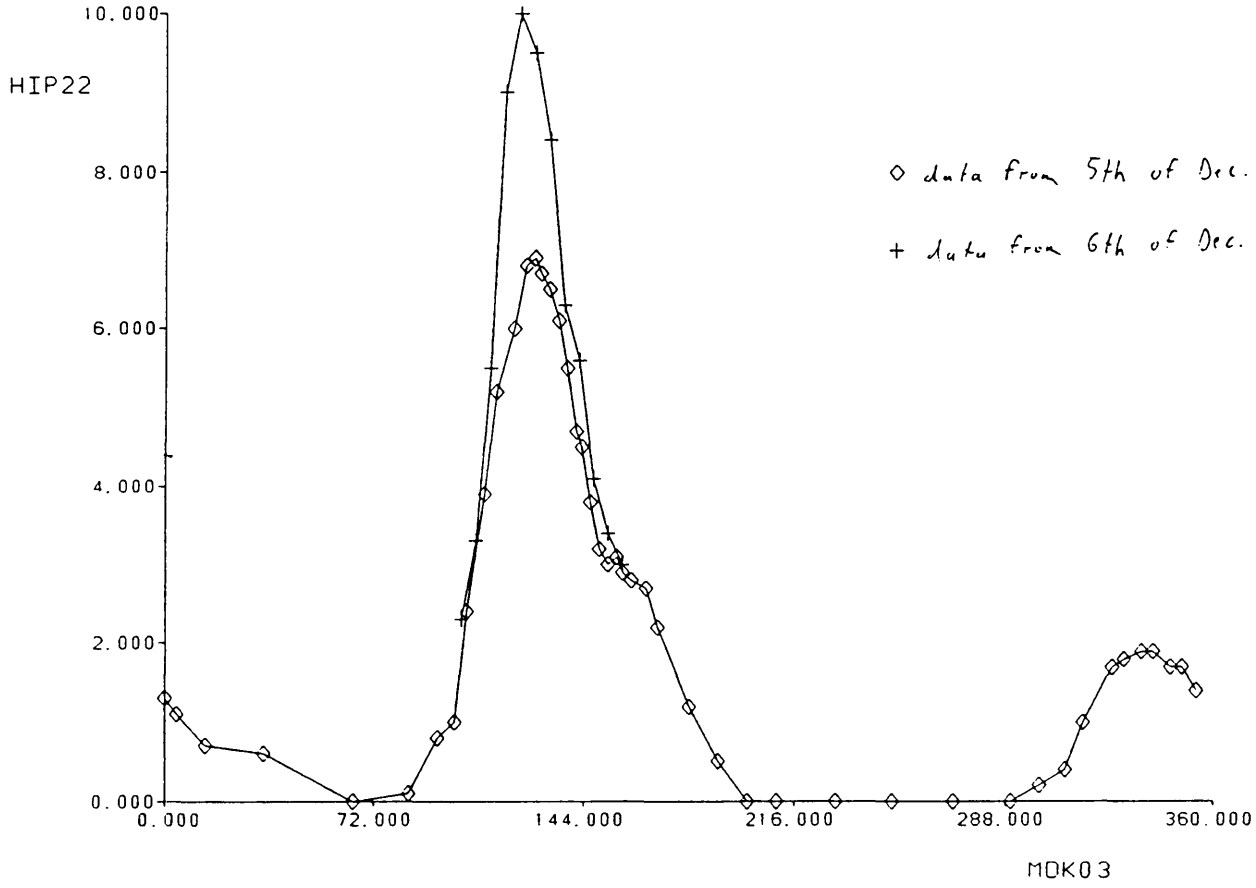

Figure 17: Dependence of energy resolved e^+ yield from the LINAC V phase.

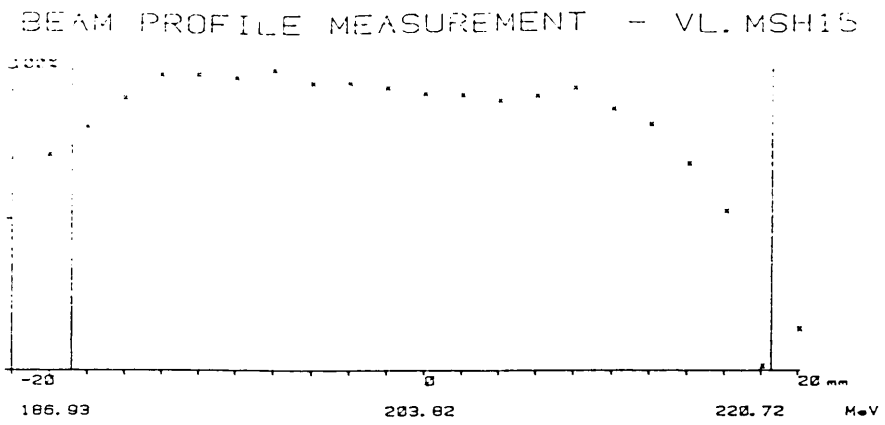

MDK03 = 100°

Central Energy 203.82 MeV
Digital Value at 100% 852 (sat. 2047)
INTENSITY (UMA meas.) -299.552 1E8 part.
Number of measurements 100

Gain is .01
Scraper VL.SLV11 (Top) : -18.8(-18.5) mm
(Bottom) : 18.5(18.5) mm

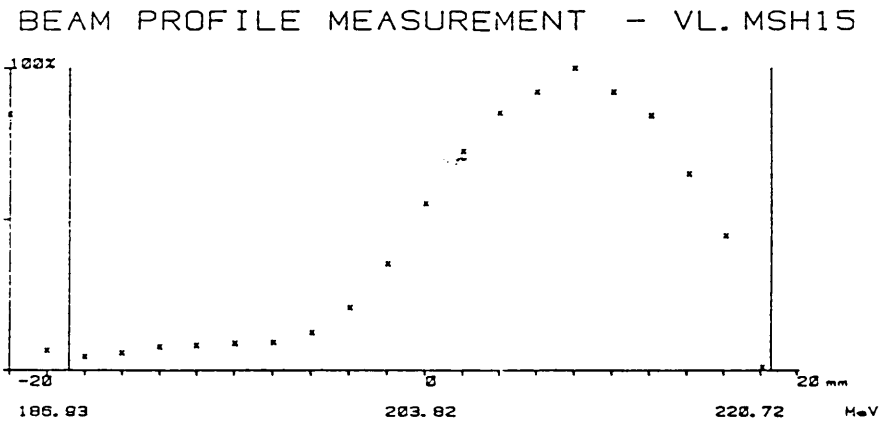

MDK03 = 110°

Central Energy 203.82 MeV
Digital Value at 100% 1295 (sat. 2047)
INTENSITY (UMA meas.) -299.552 1E8 part.
Number of measurements 100

Gain is .01
Scraper VL.SLV11 (Top) : -18.8(-18.5) mm
(Bottom) : 18.5(18.5) mm

Figure 18: The energy spectra of LINAC V for $MDK03 = 100°$ and $MDK03 = 110°$

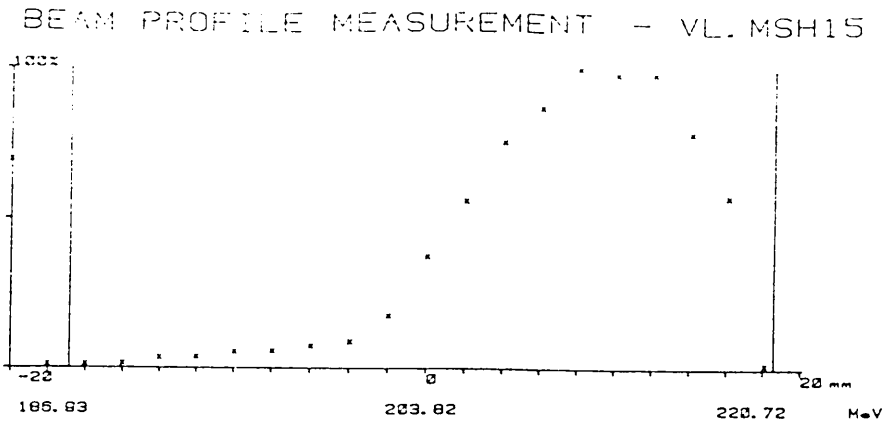

$MDK03 = 115°$

Central Energy 203.82 MeV
Digital Value at 100% 1312 (sat. 2047)
INTENSITY (UMA meas.) -298.848 1E8 part.
Number of measurements 13

Gain is .01
Scraper VL.SLV11 (Top) : -18.8(-18.5) mm
(Bottom) : 18.5(18.5) mm

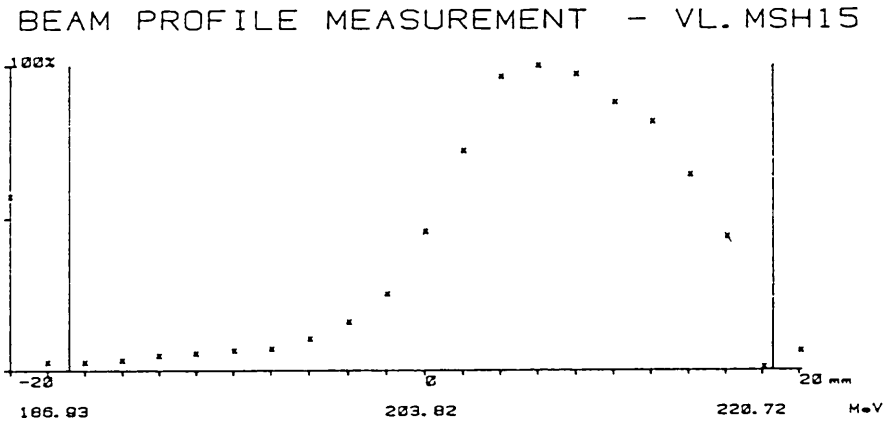

$MDK03 = 121°$

Central Energy 203.82 MeV
Digital Value at 100% 1367 (sat. 2047)
INTENSITY (UMA meas.) -300.258 1E8 part.
Number of measurements 100

Gain is .01
Scraper VL.SLV11 (Top) : -18.8(-18.5) mm
(Bottom) : 18.5(18.5) mm

Figure 19: The energy spectra of LINAC V for $MDK03 = 115°$ and $MDK03 = 121°$

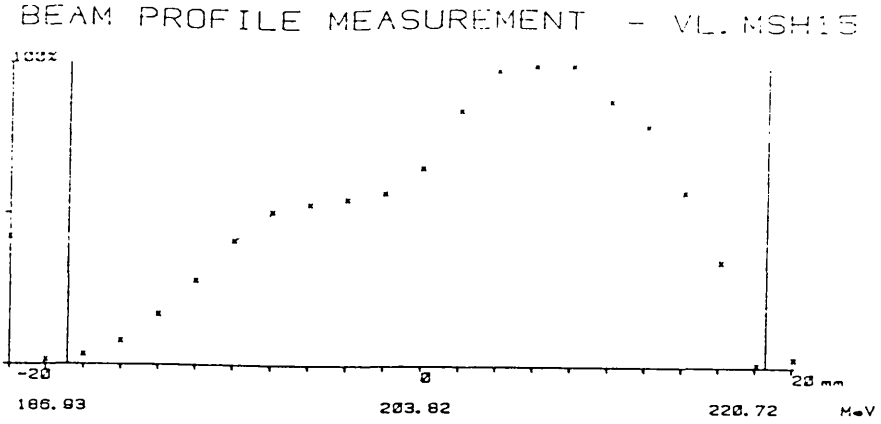

MDK03 = 131°

Central Energy 203.82 MeV
Digital Value at 100% 1229 (cal. 2047)
INTENSITY (UMA meas.) -300.258 1E8 part.
Number of measurements 13

Gain is .01
Scraper VL.SLV11 (Top) : -18.8(-18.5) mm
(Bottom) : 18.5(18.5) mm

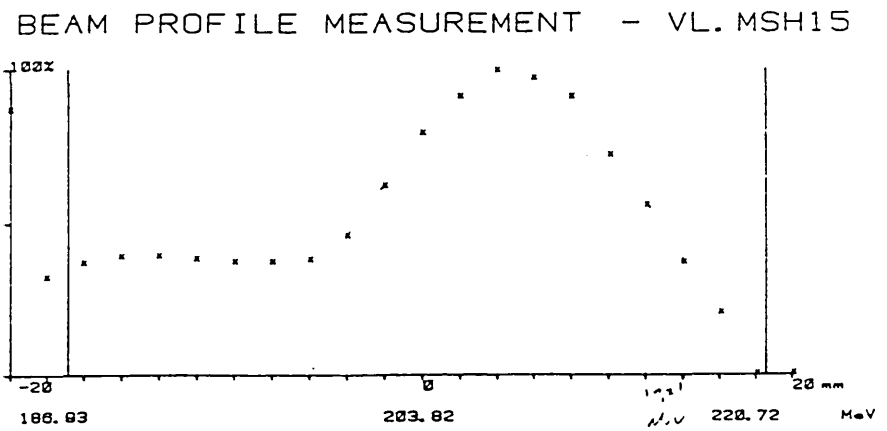

MDK03 = 135°

Central Energy 203.82 MeV
Digital Value at 100% 1248 (cal. 2047)
INTENSITY (UMA meas.) -299.552 1E8 part.
Number of measurements 13

Gain is .01
Scraper VL.SLV11 (Top) : -18.8(-18.5) mm
(Bottom) : 18.5(18.5) mm

Figure 20: The energy spectra of LINAC V for $MDK03 = 131°$ and $MDK03 = 135°$

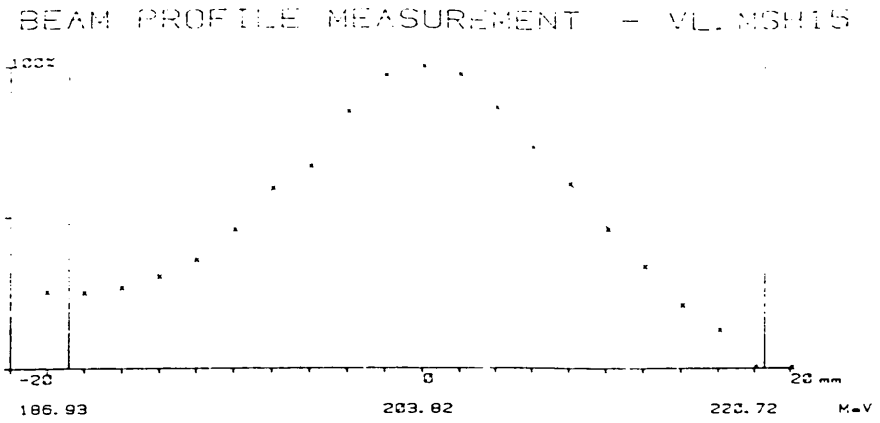

MDK03=141°

Central Energy 203.82 MeV
Digital Value at 100% 1110 (sat. 2047)
INTENSITY (UMA meas.) -300.600 1E8 part.
Number of measurements 100

Gain is .01
Scraper VL.SLV11 (Top) : -18.8(-18.5) mm
(Bottom) : 18.5(18.5) mm

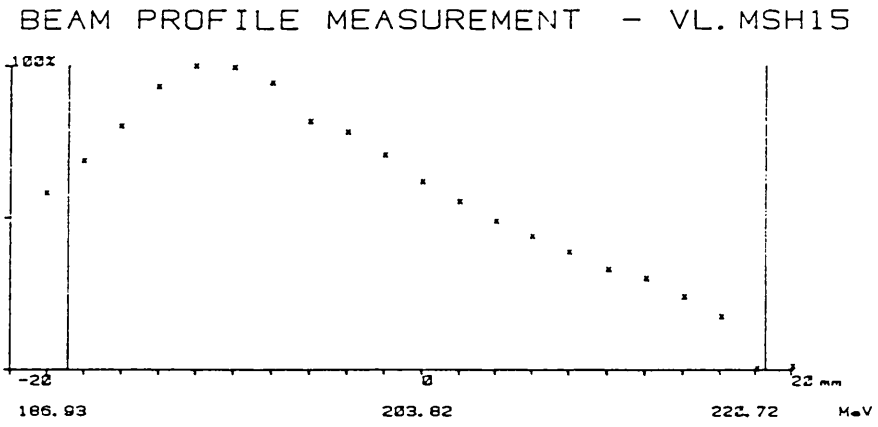

MDK03=150°

Central Energy 203.82 MeV
Digital Value at 100% 866 (sat. 2047)
INTENSITY (UMA meas.) -300.600 1E8 part.
Number of measurements 100

Gain is .01
Scraper VL.SLV11 (Top) : -18.8(-18.5) mm
(Bottom) : 18.5(18.5) mm

Figure 21: The energy spectra of LINAC V for $MDK03 = 111°$ and $MDK03 = 150°$

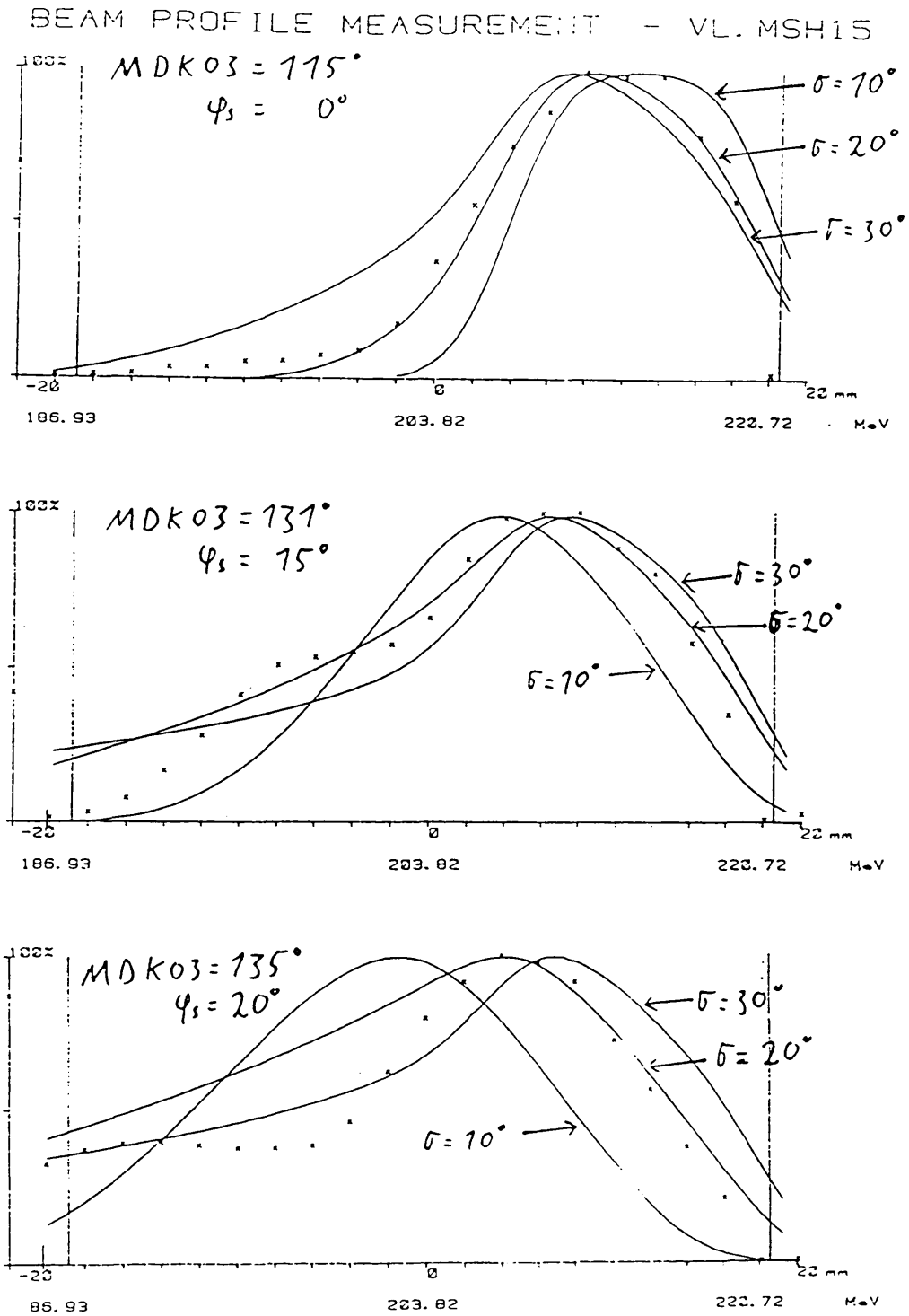

Figure 22: Comparison between calculated and measured spectra